Analysis of Lithium-ion Battery Micro-overcharge Cycle Damage Mechanism Based on Electrochemical Impedance Spectroscopy

Jingjing Zhou[1], Peipei Chao[1], Nutao Zhang[1], Peng Wang[1], Duanqian Cheng[1], Ganghui Zeng[2], Peifeng Huang[2,*]

[1] Data Center, China Automotive Engineering Research Institute Co., Ltd., Chongqing 401122, China
[2] State Key Laboratory of Advanced Design and Manufacturing for Vehicle Body, Hunan University, Changsha 410012, China

Abstract. Electrochemical impedance spectroscopy (EIS) was used to study the micro-overcharge cycle damage mechanism of Lithium-ion batteries (LIBs). Micro-overcharge cycle experiments of LIBs were carried out, and the capacity fading of LIBs under different charging cut-off voltages were analyzed. It was found that the capacity fading rate of LIBs increased with the rising of overcharge cut-off voltages and the increasing of cycle numbers. The EIS results show that the main damage pattern of LIBs during micro-overcharge cycle is the active lithium loss when the cut-off voltage is between 4.3 V and 4.4 V. Lithium loss accounts for more than 80% damage proportion when LIBs cycling for more than 20 cycles.

1 Introduction

Lithium-ion batteries (LIBs) are widely used in electronic products owing to their excellent cycling performance and high energy density. However, their safety issues have always been concerned due to the instability of the active materials. Overcharge is one of the common failure patterns of LIBs, which will destruct active materials inside LIBs, causing the capacity fading even thermal runaway.

Lots of experimental work have been done to reveal the damage mechanism of LIBs during overcharge. Zhu et al. [1] divided the process from overcharge to thermal runaway into four stages by overcharge experiments. The severe temperature rise of LIBs during overcharge was mainly originated from irreversible heat and side reactions occurred on electrodes [2]. These side reactions are usually triggered by three conditions: over-high positive potential, over-low negative potential and high temperature.

The damage mechanism of overcharged LIBs under different state of charge (SOC) has been studied by energy dispersive spectroscopy, X-ray diffraction (XRD) and electrochemical impedance spectroscopy (EIS) [3]. It was found that when the SOC of LIBs reaches 125%, lithium deposition occurs, accompanied by capacity fading, internal resistance increasing and battery swelling. The phenomenon became worse when the SOC reaches 140%, leading to destruction of cathode materials. The self-generated heat of battery became even serious when the SOC reaches 146%.

Continuous overcharge to thermal runaway is not a ubiquitous scenario for LIBs which protected by battery management systems (BMS). Whereas micro-overcharge is a more common condition for LIBs. The failure of charging devices or BMS and the inconsistency between cells will cause micro-overcharge of LIBs, which may exist for long-term along the service life. However, few studies concern the damage mechanism caused by micro-overcharge. Ouyang et al. [4] divided the overcharge process into four stages according to the capacity fading trend of LIBs, and analyzed the damage mechanism in each stage. There was no obvious capacity fading in the first stage. In the second stage, lithium accumulation loss and positive active material loss occurred, accompanied by the internal resistance increasing. In the third stage, active materials loss happened in both positive and negative electrodes, and the cell began to swell until broken in the last stage.

Herein, the damage mechanism of LIBs under micro-overcharge cycle were investigated by EIS. The influence of charging cut-off voltage on battery damage and capacity fading was also explored.

2 Experimental Sections

18650 model cells were used in the experiments, which were composed of NCM cathode and graphite anode. The normal capacity of cell was 2600 mAh. Battery test system (Neware, 5 V/12 A) was used for charge-discharge cycle test. Controlled-temperature cabinet (Lixian) was used to provide the constant temperature during the experiments. K-type thermocouple and temperature acquisition instrument were used to monitor the cell temperature. EIS spectra were obtained by electrochemical analyzer. In order to obtain the actual capacity of the cells that undergo multiple micro-overcharge cycles, overcharge-discharge and normal charge-discharge were conducted alternately, as shown in Figure 1.

The pretreated cells were allocated to 12 groups (Table 1) for the follow-up micro-overcharge cycle test, as shown in Table 1. Constant current/voltage charge and constant

* Corresponding author: pfhuang@hnu.edu.cn

current discharge were adopted for both micro-overcharge and normal charge cells, and the discharge cut-off voltage was 2.75 V. In order to reduce the polarization effect, 30 min rest was set between each charge and discharge process.

Table 1. Experimental parameters in micro-overcharge cycle.

Group	Charging cut off voltage	Charging rate
1, 2	4.25 V	1 C
3, 4	4.3 V	1 C
5, 6	4.35 V	1 C
7, 8	4.4 V	1 C
9, 10	4.5 V	1 C
11, 12	4.6 V	1 C

EIS test was determined in the frequency range from 10 kHz to 0.1 Hz in the experiment intermittently. Every 20 cycles were applied for the groups with low cut-off voltage and charging rate (group 1-6). Every 10 cycles were applied for the groups with higher cut-off voltage and charging rate (group 7-12). Micro-overcharge cycle was terminated when the actual capacity fell below 70% of the initial normal capacity. All the experiments were conducted at 30 °C. The flow chart of the experiment is shown in Figure 1.

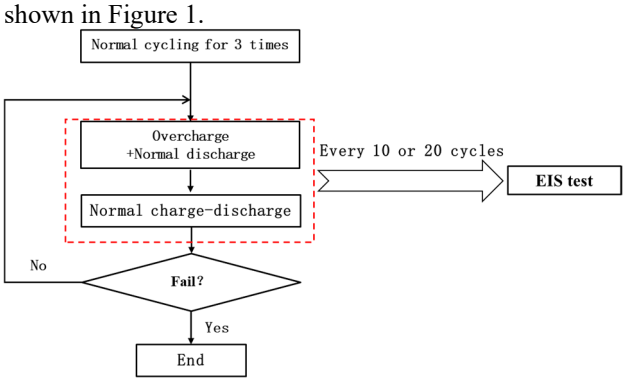

Fig. 1. Flow chart of micro-overcharge cycle experiment.

3 Analysis of capacity fading

The capacity fading curves of each group in the micro-overcharge cycling test are summarized in Figure 2, in which one cycle contains overcharge-discharge-charge-discharge four steps. It is clear that the capacity fading rate of cells accelerated with the cycle numbers increasing. Besides, the cycle number corresponding to cell failure decreases with the increase of charging cut-off voltage. The cycle number of cell failure is the least when the cut-off voltage is 4.6 V, which are 23 and 22 respectively. It is worth noting that when the cut-off voltage is 4.4 V or above, the capacity fading rate increases obviously. This may be related to the manganese dissolution reaction started from 4.35 V. The 4.4 V high potential leads to the loss of active material in positive, resulting in the accelerated capacity fading of cells.

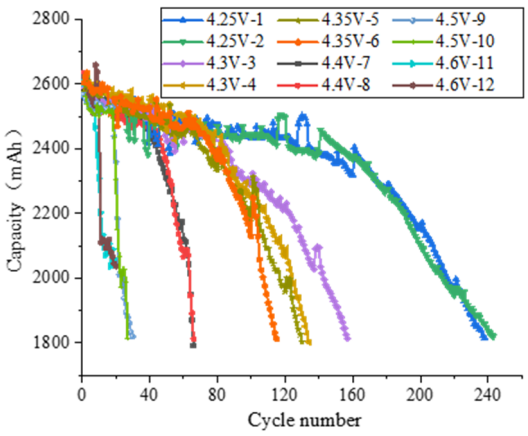

Fig. 2. Capacity fading data during micro-overcharge cycles of groups.

4 Damage mechanism of LIBs during micro-overcharge cycle

The damage mechanism of LIBs can be classified as forced internal short circuit, spontaneous internal short circuit, loss of lithium Inventory (LLI), loss of active materials (LAM) and loss of conduction (LoC). LLI and LAM mainly refer to the loss of transportable lithium and active materials used for charge and discharge processes. LLI is related to the decomposition and regeneration of solid electrolyte interphase (SEI), the conversion of 'active lithium' to 'dead lithium' during lithium deposition, the growth of lithium dendrite and the side reaction between lithium and electrolyte. LAM is related to the destruction of crystal structure, the decomposition of active materials, the reduction of crystal interface, the reaction between active materials and deposited lithium, and the exfoliation of materials. LoC is mainly reflected as dissolution of copper collector or the decomposition of adhesive in anodes, corrosion of aluminum collector in cathode [5]. These three damage patterns are the main factors leading to the capacity degradation.

Typical EIS spectra are usually represented by Nyquist diagrams (Figure 3), the horizontal axis and the longitudinal axis represent the real part and imaginary part of impedance respectively. A typical EIS spectrum can be separated into three regions from high frequency to low frequency. The high frequency region contains a small semicircle, which represents the migration of lithium ions through SEI. The medium frequency region contains a large semicircle, which represents the charge transfer process. While the low frequency region contains a straight line with a slope of 1, which reflects the diffusion process of lithium ions and is characterized by Warburg impedance. In addition to the above three regions, the intercept of Nyquist diagram on the horizontal axis indicates the ohmic impedance R_{ohm} [6].

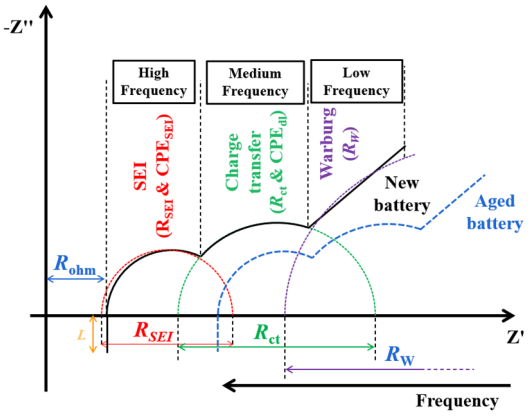

Fig. 3. Typical EIS spectra of LIBs.

Critical impedance parameters (ohmic impedance R_{ohm}, SEI impedance R_{SEI}, charge transfer impedance R_{ct} and Warburg impedance R_w) can be obtained by using equivalent circuit model to fit the EIS spectrum. The damage mechanism of LIBs can be quantitatively studied by investigate the change trend of impedance parameters with cycle numbers. The equivalent circuit model used in this work is shown in Figure 4.

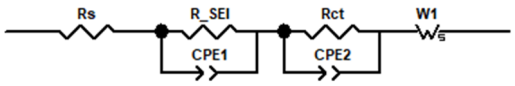

Fig. 4. Equivalent circuit model.

Damage patterns of LIBs can be revealed by different impedance change forms. R_{ohm} represents the overall ohmic impedance of collector, binder, electrolyte and separator in LIBs. When the cell is constantly damaged, the collector will be corroded, the binder will decompose, and the composition of the electrolyte will be changed [7]. Those changes will lead to the increase of R_{ohm}, which is a major sign of LoC. On the other hand, SEI will decompose and reform continuously during the process of damage. Its properties, composition and thickness change correspondingly, resulting in the increase of R_{SEI} [7]. Meanwhile, the changes of SEI hinder the transportation of lithium ion between electrolyte and anode, leading to irreversible loss of lithium ion. Therefore, the increase of R_{SEI} is a sign of LLI. In addition, the growth of lithium dendrite and the blockage of micropores in separator are two important causation for LLI. The above two changes will also induce the decrease of charge transfer (lithium ions de-intercalation in cathode and anode), which leading to the increase of R_{ct} [7]. Thus, the increase of R_{ct} is closely related to LLI as well. R_w is related to the effective diffusion path length, which is closely infected by the electrode form. LAM will cause the change of electrode form (such as the decrease of pore size), and eventually lead to the increase of R_w. Based on the corresponding relationship between impedance and damage pattern, the contribution of different damage patterns at different stages can be calculated according to equations (1) - (7).

$$LoC_{C=n}^{SOC=100\%} = \frac{Rohm_{C=n}^{SOC=100\%} - Rohm_{C=0}^{SOC=100\%}}{Rohm_{C=0}^{SOC=100\%}} \quad (1)$$

$$LLI_{C=n}^{SOC=100\%} = \frac{R_{SEI\,C=n}^{SOC=100\%} - R_{SEI\,C=0}^{SOC=100\%}}{R_{SEI\,C=0}^{SOC=100\%}} + \frac{R_{ct\,C=n}^{SOC=100\%} - R_{ct\,C=0}^{SOC=100\%}}{R_{ct\,C=0}^{SOC=100\%}} \quad (2)$$

$$LAM_{C=n}^{SOC=100\%} = \frac{R_{w\,C=n}^{SOC=100\%} - R_{w\,C=0}^{SOC=100\%}}{R_{w\,C=0}^{SOC=100\%}} \quad (3)$$

$$Total_{C=n}^{SOC=100\%} = LoC_{C=n}^{SOC=100\%} + LLI_{C=n}^{SOC=100\%} + LAM_{C=n}^{SOC=100\%} \quad (4)$$

$$LoC\%_{C=n}^{SOC=100\%} = \frac{LoC_{C=n}^{SOC=100\%}}{Total_{C=n}^{SOC=100\%}} \times 100\% \quad (5)$$

$$LLI\%_{C=n}^{SOC=100\%} = \frac{LLI_{C=n}^{SOC=100\%}}{Total_{C=n}^{SOC=100\%}} \times 100\% \quad (6)$$

$$LAM\%_{C=n}^{SOC=100\%} = \frac{LAM_{C=n}^{SOC=100\%}}{Total_{C=n}^{SOC=100\%}} \times 100\% \quad (7)$$

Figure 5 (a)-(c) shows the comparison of experimental and fitted EIS in the three experimental cell groups (group 4, 6 and 8). The change trend of R_{ohm} in the first 60 cycles is not obvious for group 4, indicating that LoC damage pattern is not significant during this period. R_{ohm} increases gradually after 80th cycle, and the trend becomes apparently, while R_{ohm} increases generally for the other two groups. Besides, two semicircles of EIS curve expand with the increasing of cycle numbers, but the second semicircle expands more obviously. This means that the SEI grows slowly and the charge transfer process declines obviously during the micro-overcharge cycle. Therefore, the change of R_{SEI} is not obvious, while the R_{ct} increases rapidly. The change trend of R_w can not be accurately obtained from EIS curve alone, and quantitative mean is needed.

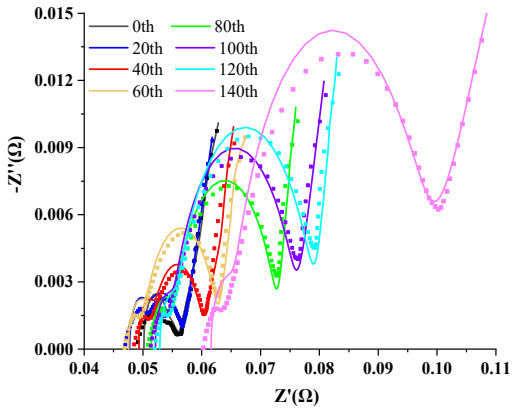

a) The fitted EIS curves of group 4 (4.3 V)

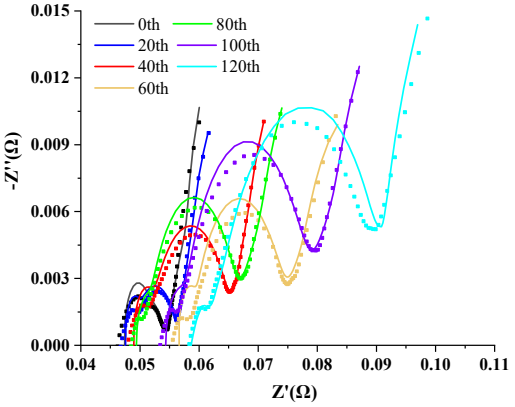

b) The fitted EIS curves of group 6 (4.35 V)

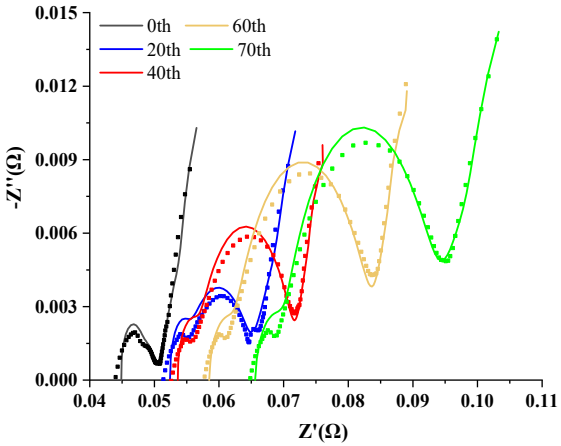

c) The fitted EIS curves of group 8 (4.4 V)

Fig. 5. Comparison of experimental and fitted EIS in the three experimental groups (solid lines are fitted data, dots are experimental data).

Equivalent circuit is used to fit the EIS curves of the three experimental groups (4, 6 and 8). Damage pattern analysis results are shown in Figure 6. It is obvious that LLI accounts for the largest proportion in damage patterns among all the three groups (Figure 6a-c). To be specific, the proportions of LLI are about 90%, 80%-90% and 60%-90% in group 4, 6 and 8, respectively. The proportions of LAM and LoC are about 0%-20% for all three groups. This indicates that LLI is the main failure mechanism for the micro-overcharge cycle with the cut-off voltage between 4.3 V and 4.4V, followed by LAM and LoC.

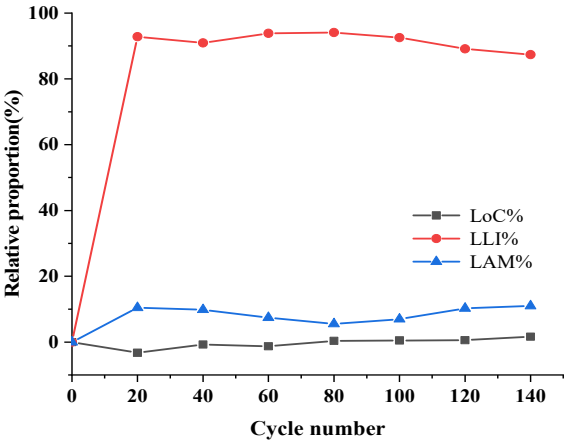

a) Proportion of damage patterns in experimental group 4 (4.3 V)

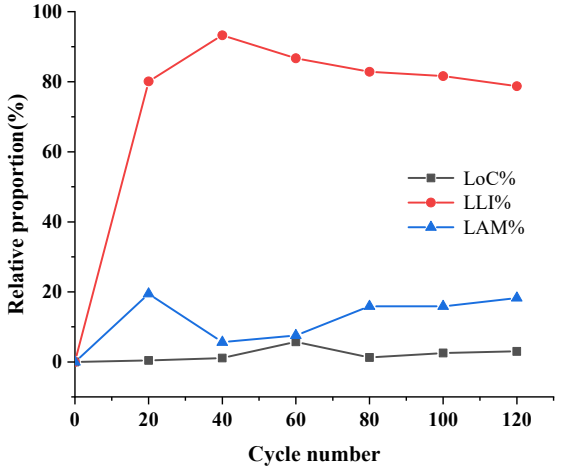

b) Proportion of damage patterns in experimental group 6 (4.35 V)

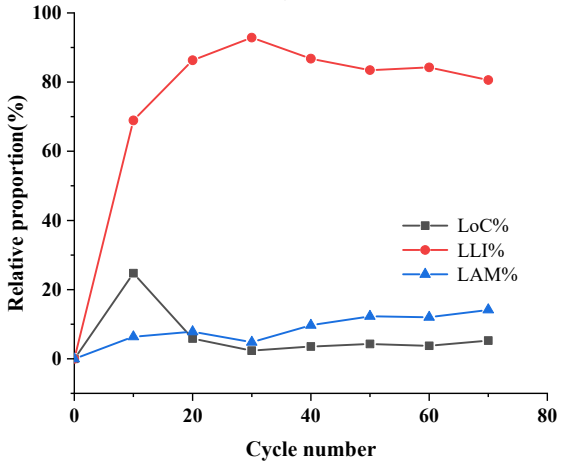

c) Proportion of damage patterns in experimental group 8 (4.4 V)

Fig. 6. Impedance and proportion of damage patterns in the three groups.

5 Conclusion

In this study, the capacity fading of LIBs was investigated based on the experimental capacity data. It was found that the capacity fading rate of LIBs increased with the increasing of cycle numbers. The turning points of capacity changes at different cut-off voltages, and the capacity difference becoming larger, which can be used as the basis for fault diagnosis. Through the analysis of EIS curves, it is shown that the main damage pattern of LIBs during micro-overcharge cycle is LLI, followed by LAM and LoC for the battery with the charge cut-off voltage between 4.3 V and 4.4 V. When LIBs cycle for more than 20 cycles, the damage proportion of LLI accounts for 80% ~ 90%.

Acknowledgments

This study was financially supported by the National Key Research and Development Program of China (No. 2019YFB1600800) and the Natural Science Foundation of Hunan Province (No. 2020JJ5060).

References

1. X. Zhu, Z. Wang, Y. Wang, H. Wang, C. Wang, L. Tong, et al. Overcharge investigation of large format lithium-ion pouch cells with $Li(Ni_{0.6}Co_{0.2}Mn_{0.2})O_2$ cathode for electric vehicles: Thermal runaway features and safety management method. Energy. 169 (2019) 868-80.
2. Y. Zeng, K. Wu, D. Wang, Z. Wang, L. Chen. Overcharge investigation of lithium-ion polymer batteries. J Power Sources. 160 (2006) 1302-7.
3. Y. Liu, R. Huo, H. Qin, X. Li, D. Wei, T. Zeng. Overcharge investigation of degradations and behaviors of large format lithium ion battery with $Li(Ni_{0.6}Co_{0.2}Mn_{0.2})O_2$ cathode. Journal of Energy Storage. 31 (2020) 101643.
4. M. Ouyang, D. Ren, L. Lu, J. Li, X. Feng, X. Han, et al. Overcharge-induced capacity fading analysis for large format lithium-ion batteries with $Li_yNi_{1/3}Co_{1/3}Mn_{1/3}O_2 + Li_yMn_2O_4$ composite cathode. Journal of power sources. 279 (2015) 626-35.
5. C. Pastor-Fernández, W.D. Widanage, J. Marco, M.-Á. Gama-Valdez, G.H. Chouchelamane. Identification and quantification of ageing mechanisms in Lithium-ion batteries using the EIS technique. 2016 IEEE Transportation Electrification Conference and Expo (ITEC). IEEE2016. pp. 1-6.
6. A. Barai, G.H. Chouchelamane, Y. Guo, A. McGordon, P. Jennings. A study on the impact of lithium-ion cell relaxation on electrochemical impedance spectroscopy. Journal of Power Sources. 280 (2015) 74-80.
7. J. Vetter, P. Novák, M.R. Wagner, C. Veit, K.-C. Möller, J. Besenhard, et al. Ageing mechanisms in lithium-ion batteries. Journal of power sources. 147 (2005) 269-81.